Chemosphere 375 (2025) 144252

Contents lists available at ScienceDirect

Chemosphere

journal homepage: www.elsevier.com/locate/chemosphere

Development of novel biochar adsorbent using agricultural waste biomass for enhanced removal of ciprofloxacin from water: Insights into the isotherm, kinetics, and thermodynamic analysis

Bablu Alawa [a], Surya Singh [a,b,*], Sankar Chakma [c], Rupak Kishor [d], Cecilia Stålsby Lundborg [e], Vishal Diwan [a,e,f,**]

[a] Division of Environmental Monitoring and Exposure Assessment (Water & Soil), ICMR – National Institute for Research in Environmental Health (NIREH), Bhopal, 462 030, India
[b] Faculty of Biological Sciences, Academy of Scientific and Innovative Research (AcSIR), Ghaziabad, 201 002, India
[c] Department of Chemical Engineering, Indian Institute of Science Education and Research (IISER) Bhopal, Bhopal, 462 066, India
[d] Department of Chemical Engineering, Maulana Azad National Institute of Technology (MANIT), Bhopal, 462 003, India
[e] Department of Global Public Health, Karolinska Institutet (KI), Stockholm, 171 77, Sweden
[f] Faculty of Medical Sciences, Academy of Scientific and Innovative Research (AcSIR), Ghaziabad, 201 002, India

HIGHLIGHTS

- Removal of CIP from water was studied using agricultural waste derived biochar.
- Activated biochar prepared from wheat straw was capable to remove ~98% of CIP.
- Interaction between activated biochar and CIP enhanced adsorption capacity by 36–44%.
- Minimal effect of temperature was seen during adsorption of CIP using adsorbents.
- Pore filling and surface adsorption mechanism prevail during CIP adsorption.

GRAPHICAL ABSTRACT

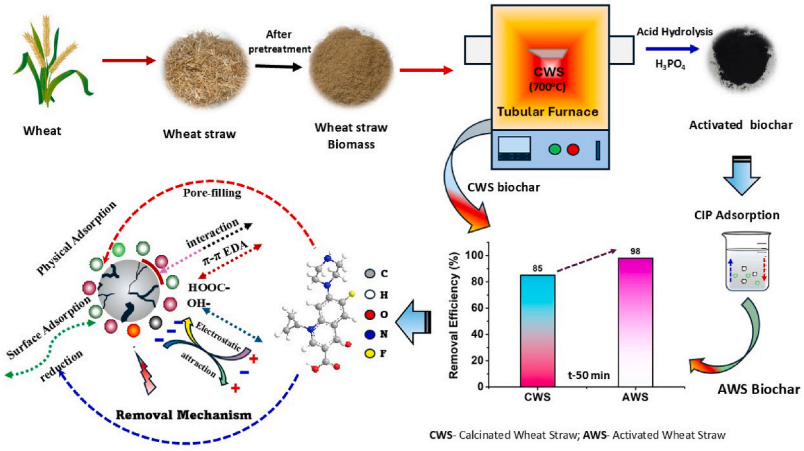

ARTICLE INFO

Handling editor: Yongmei Li

ABSTRACT

Increase in the antibiotic's usage and mis-management in antibiotics' disposal has led to the occurrence of antibiotic residues in the surface water bodies. These residues may pose considerable risks to the human as well

* Corresponding author. Division of Environmental Monitoring and Exposure Assessment (Water & Soil), ICMR – National Institute for Research in Environmental Health (NIREH), Bhopal, 462 030, India.
** Corresponding author. Division of Environmental Monitoring and Exposure Assessment (Water & Soil), ICMR – National Institute for Research in Environmental Health (NIREH), Bhopal, 462 030, India.
E-mail addresses: suryasingh.nireh@icmr.gov.in (S. Singh), vishal.diwan@ki.se, vishal.diwan@icmr.gov.in (V. Diwan).

https://doi.org/10.1016/j.chemosphere.2025.144252
Received 26 November 2024; Received in revised form 30 January 2025; Accepted 20 February 2025
Available online 27 February 2025

Keywords:
Adsorption
Antibiotic
Antimicrobial resistance
Ciprofloxacin
wheat straw biochar
Langmuir isotherm

as aquatic organisms owing to the enhancement in antimicrobial resistance among microbes. Hence, precautionary measures are need of the hour to curtail the occurrence of antibiotic compounds in water. In addition, rampant burning of agricultural waste in India causes considerable air pollution. Considering this, a novel adsorbent has been developed from agricultural waste biomass, *viz.* wheat straw (WS), through calcination (CWS), followed by chemical activation (AWS). These adsorbents were employed for the removal of ciprofloxacin (CIP) from water. Removal efficiency of 90% (for CWS) and 98% (for AWS) could be achieved at neutral pH in room temperature conditions. The maximum adsorption capacity of ciprofloxacin on synthesized adsorbent was evaluated as 14.51 mg g^{-1}. Experimental findings were further explored to get the insights of isotherm, kinetics, and thermodynamics involved in the process. It was found that Langmuir model (with R^2 value of 0.985) provided a better fit than the other isotherm models. Kinetics and thermodynamic studies revealed that adsorption process followed the pseudo second order linear kinetic model (with R^2 value of 0.999) with endothermic and spontaneous sorption of ciprofloxacin on developed adsorbent. Thus, wheat straw waste may suitably be used as adsorbent for the removal of antibiotics from water.

1. Introduction

Antibiotics are one of the life-saving medicines that have helped increasing survival and longevity (Hutchings et al., 2019). Considering their efficacy, antibiotic consumption is projected to surge globally, with estimates indicating a 67% increase by 2030 (One Health Trust, 2015). This upward trend underscores escalating reliance on antibiotics across sectors, posing future challenges for public health and environmental sustainability (Gahrouei et al., 2024). The antibiotics consumed by humans and animals do not completely metabolize and enter into the environment though excretion. Further, disposal of expired medications from various sources and runoff from pharmaceutical manufacturing and veterinary establishments also contribute to the phenomena of antimicrobial resistance in environment (Bilal et al., 2020; Oharisi et al., 2023; Alawa et al., 2024). As per the WHO report, global antibiotic use among patients soared during the COVID-19 pandemic, reaching up to 83% in some regions despite only 8% of patients actually needing them for bacterial co-infections. Such overuse of antibiotics, especially higher-resistance 'Watch' category ones, posed significant risks, exacerbating antimicrobial resistance without improving clinical outcomes for COVID-19 patients (WHO, 2024).

The increasing prevalence of antibiotics in aquatic environment has raised concerns about their potential adverse effects on ecosystems and human health (Parashar et al., 2022). Among these, ciprofloxacin (CIP), a broad-spectrum antibiotic, is a crucial pharmaceutical compound which is extensively utilized globally. It falls under the category of fluoroquinolones (FQ), serving both human and veterinary medical needs (Azzam et al., 2022; Oliveira et al., 2023). CIP has been detected in various water bodies globally with detection rates exceeding 50% due to extensive usage (Peñafiel et al., 2021; Jara-Cobos et al., 2023; Jiang et al., 2024). The concentrations vary widely, ranging from nanograms per liter (ng/L) to micrograms per liter (μg/L) (Ricky and Shanthakumar, 2023; Oharisi et al., 2023). According to the findings of National Centre for Disease Control (NCDC), resistance to CIP was observed in 60–68% of all tested specimens (NCDC, 2023; Singh et al., 2024a). Due to its persistence, bioaccumulation potential, and adverse impacts on non-target organisms, the removal of CIP from water sources has become a critical environmental challenge (Wang et al., 2020).

Hence, it is crucial to develop treatment technologies capable of removing antibiotics, having long persistence time, from surface and wastewater systems. To deal with these issues, several physicochemical techniques have been used for the removal of ciprofloxacin, such as, advanced oxidation process (AOP), membrane separation, adsorption, microbial electrolysis ultraviolet cell (MEUC), UV/H_2O_2/O_3 degradation, and photocatalytic degradation (Xue et al., 2022; Al-Buriahi et al., 2022). However, these methods have their own merits and demerits depending on various parameters such as cost, time, and their toxic byproducts (Igwegbe et al., 2021; Qalyoubi et al., 2022). Scientific communities are investigating efficient technology for the removal of CIP from water bodies (Kusworo et al., 2024; Barzegar et al., 2023; Pham et al., 2024; Le et al., 2024; Khan et al., 2024a). In recent years, biochar has emerged as a promising adsorbent for the removal of antibiotics from water due to its high surface area, porous structure, and surface functionality (Suliman et al., 2017; Feng et al., 2021; Leng et al., 2021; Venkatachalam et al., 2023). Biochar is a carbonaceous material produced from the pyrolysis of biomass under controlled conditions. Its unique properties make it an effective sorbent for a wide range of contaminants, including antibiotics (Ahmad et al., 2014). Several studies have demonstrated the effectiveness of biochar in removing CIP from aqueous solutions (Wang et al., 2020; Yu et al., 2020). Additionally, biochar offers the advantage of being a sustainable and cost-effective solution for water treatment, as it can be produced from a variety of feedstocks, such as agricultural residues, forestry waste, and organic byproducts.

In this investigation, the adsorptive removal of CIP using wheat straw agricultural waste has been explored. Wheat straw waste has been purposely selected as it is generally burned in India to clean-up the agricultural land, also known as 'stubble burning', and thus results in considerable air pollution (Lan et al., 2022; Govardhan et al., 2023). Therefore, application of wheat straw as an adsorbent would not only help in removal of antibiotics from water; but would also contribute in mitigating the air pollution. Having this concept, the wheat straw waste was treated to develop biochar adsorbent. The effects of various parameters such as pH, contact time, initial concentration of antibiotic, adsorbent dose, and temperature for the optimization of process have been studied. The kinetics, isotherms, and thermodynamic parameters were also calculated to explore the mechanism involved in CIP adsorption onto the biochar surface.

2. Materials and method

2.1. Materials

Agricultural waste biomass *i.e.* wheat straw (WS) was collected from the farms near to the ICMR-NIREH campus at Bhauri, Bhopal, India. The ciprofloxacin, ethanol, and phosphoric acid (H_3PO_4) were procured from Merck life science, Merck, and Molychem, respectively. MiliQ water was used in all the experiments.

2.2. Synthesis of biochar and activated biochar using agricultural waste

The raw wheat straw material collected from agricultural field was sundried for a period of 5 d. The material was washed with water to remove the dust particles and dried in a hot air oven (*Make:* BVSE India) at 65 °C for 48 h. The dried material was cooled down to room temperature and used for size reduction using Lab blender (*Make:* Lab Smith). The converted powder was screened using different mesh sizes. In the current investigation, 300-μm size particles were used for experiments. The obtained biomass (Wt. 2 g of 300-μm particle size) was pyrolyzed in tubular furnace (*Make:* Exacta) at 700 °C with the heating rate of 10 °C/min. The holding time for each set of the experiment was taken as 2 h at the specified reaction temperature. The flow rate of N_2

was maintained in the range of 200–300 ml/min. The pyrolyzed sample was washed several times with water to remove soluble impurities followed by drying in hot air oven at 110°C for 24 h. The dried sample, *viz.* calcined wheat straw (CWS) was collected, weighed, and stored for further characterization. The process flow diagram for the synthesis of adsorbent is shown in Fig. 1.

The prepared CWS sample was used for the activation using phosphoric acid. The calcined sample was washed with water to remove the dirt and impurities and dried at 110°C for 24 h. The CWS sample was further activated using H_3PO_4 at the ratio of 1:3 (CWS: H_3PO_4) through dry impregnation method at 105 °C for 48 h. After drying, the sample was calcined at 700°C with heating rate of 10 °C/min and 2 h holding time. The flow of nitrogen during the calcination was maintained at 200 ml/min till cooling. After cooling, the activated biochar sample, *viz.* activated wheat straw (AWS), was rinsed with water till neutral pH was obtained. All samples were further dried at 115 °C for 24 h and crushed to desired size to get the final adsorbent. All adsorbents were stored in airtight containers to avoid moisture exposure (Fig. 1).

2.3. Characterization of synthesized adsorbents

The prepared adsorbents were characterized using different analytical techniques. The surface morphology and chemical composition of the agricultural waste biomass derived biochar and activated biochar were determined using Field Emission-Scanning Electron Microscopy (FESEM) (Make: Zeiss, Model: ULTRA Plus) coupled with Energy Dispersive X-ray spectrometer (EDX). The identification of the functional group on the biochar surface was determined using Fourier transform infrared (FTIR) spectrometry (Make: Shimadzu, Model: Affinity-1S) in the frequency range of 400–4000 cm^{-1}. The structural analysis of biochar was analyzed using powder X-ray Diffraction (P-XRD) (Make: PANalytical, Model: Empyrean) in the range of 10–90° at 2 theta value. The biomass characteristics and its thermal behavior have been analyzed using thermo-gravimetric analysis (TGA) (Make: PerkinElmer, Model: TGA 4000).

2.4. Adsorption study of ciprofloxacin

The concentration of CIP was analyzed using UV (Ultraviolet) spectroscopy (Make: Shimadzu; Model: 1800). Several batch experiments were carried out to investigate the CIP removal capacity of WS derived biochar *viz.* CWS and AWS. The 10 mgL^{-1} initial concentration of the CIP solutions were prepared. The initial dose of adsorbent was used as 1.0 gL^{-1} in each case. Conical flasks were placed in orbital shaker at 150 ± 1 rpm for a contact time of 240 min. After this, CIP solution was filtered through 0.45 μm syringe filter for further analysis at wavelength of 277 nm using spectrophotometer. Adsorption capacity (q_e in $mg.g^{-1}$) and removal efficiency (R in %) of the adsorbents were calculated using equations (1) and (2), respectively (Xue et al., 2022; Pham et al., 2024):

$$q_e = \frac{(C_o - C_e)}{m} \times V \quad (1)$$

$$\% R = \frac{(C_o - C_e)}{C_o} \times 100 \quad (2)$$

where, C_o and C_e are the initial and residual equilibrium concentration of adsorbate in $mg{\cdot}L^{-1}$, respectively. V is the total volume of solution used in L during the experiment; and m is the mass of adsorbent in g.

The adsorption of CIP on synthesized adsorbents was studied under variable conditions to obtain the optimized reaction parameters in order to achieve the highest removal efficiency. The optimized set of conditions were further used for studying the kinetics, isotherms, and thermodynamics of the adsorption process. The effect of pH on the adsorption of CIP was determined by varying the pH from 1.0 to 13.0 with the help of 0.1 M NaOH and 0.1 M HNO_3 solutions keeping other parameters constant. The adsorbent (WS/CWS/AWS) dose was varied from 0.2 to 1.8 gL^{-1} for adsorption of CIP keeping the initial CIP concentration at 10 mgL^{-1}. After obtaining the optimized dose of synthesized adsorbents, CIP concentration was varied in the range of 1.0–30.0 mgL^{-1}. The reaction was also undertaken at different contact times, *viz.* 5, 10, 20, 30, 40, 50, 60, 90, 120, 240 min, for kinetic studies. Thermodynamic studies were conducted in the temperature range of

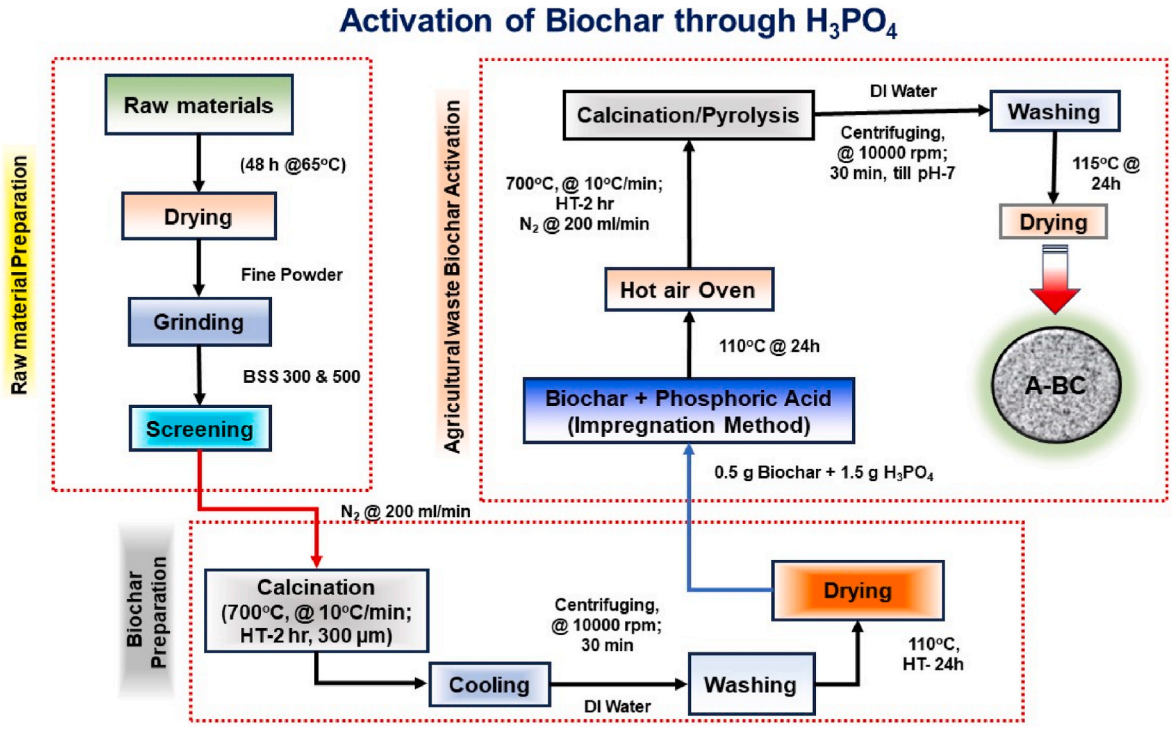

Fig. 1. Schematic diagram for synthesis of wheat straw derived calcined (CWS) and activated (AWS) biochar.

5–45 °C. All experiments were performed after shaking the reaction solution at 150 rpm. The CIP concentration after each of these experiments was determined using UV–Vis Spectroscopy using fixed wavelength of 277 nm.

2.5. Adsorption kinetics

The adsorption of CIP using WS derived biochar as CWS and AWS was determined using linear and non-linear kinetic models *viz.* pseudo first order (PFO), pseudo second order (PSO), Intra particle diffusion model, Elovich model and Liquid – Film model, as shown in Eqs. (1)–(8) of Table S1 (López-Luna et al., 2019; Hamadeen and Elkhatib, 2022; Arif et al., 2022).

2.6. Adsorption isotherms

The isotherm models, such as Langmuir (Alnajrani and Alsager, 2020), Freundlich (López-Luna et al., 2019), Dubinin-Radushkevitch (D-R) (Jara-Cobos et al., 2023), and Temkin model (Al-Fawwaz et al., 2023) were studied to understand the interaction mechanisms and to identify the suitable model which accurately fits the adsorption data and provides valuable information regarding this interaction between adsorbate and adsorbent. Adsorption isotherms elucidate both the adsorption capacity and the concentration of the adsorbate, establishing an equilibrium correlation between the two. The uniformity of the adsorbent surface implies an equal energy of adsorption across all active sites, devoid of any intermolecular interactions (Laishram et al., 2022).

Langmuir Isotherm: It describes the type of physical adsorption as monolayer adsorption (Saadi et al., 2015). The nonlinear model is expressed in equation (3), whereas the linear form of model is presented in equation (4) (Pham et al., 2024; Le et al., 2024; Alnajrani and Alsager, 2020)

$$q_e = \frac{q_m k_L C_e}{1 + k_L C_e} \tag{3}$$

$$\frac{C_e}{q_e} = \frac{C_e}{q_m} + \frac{1}{k_L q_m} \tag{4}$$

Where, q_e = Amount of adsorbate adsorbed at equilibrium time ($mg{\cdot}g^{-1}$), q_m = Maximum amount of adsorbate adsorbed ($mg{\cdot}g^{-1}$), k_L = Langmuir model constant, C_e = Concentration of adsorbate at equilibrium time (mgL^{-1}).

The behavior of the adsorption of CIP can be evaluated using the dimensionless separation factor R_L, representing a significant characteristic of the Langmuir model as shown in equation (5) (Laishram et al., 2022)

$$R_L = \frac{1}{1 + k_L q_m} \tag{5}$$

Value of R_L lies between 0 and 1, where it indicates irreversible isotherm if $R_L = 0$, favorable if the value lies between $0 < R_L < 1$, linear nature if $R_L = 1$ and, unfavorable behavior of reaction if $R_L > 1$ (Alnajrani and Alsager, 2020; Al-Fawwaz et al., 2023).

Freundlich Isotherm: According to this model, quantity of adsorbate adsorbed on the exterior surface of adsorbent is directly proportional to pressure of gas. The isotherm equation is expressed as (López-Luna et al., 2019)

$$q_e = k_F C_e^{1/n} \tag{6}$$

where, q_e = Amount of adsorbate adsorbed at equilibrium time (mgg^{-1}), k_F = Freundlich affinity coefficient $(\mu\text{-mol}g^{-1})/(\mu\text{-mol}L^{-1})^{1/n}$, C_e = Concentration of adsorbate at equilibrium time (mgL^{-1}), 1/n = Freundlich exponential index.

Dubinin-Radushkevitch (DR) Isotherms: This isotherm gives information regarding the physical and chemical adsorption and apparent energy of adsorption as shown in equation (7) (Jara-Cobos et al., 2023; Dolfini et al., 2024)

$$q_e = q_m \exp\left[-k_D \left\{ RT \ln\left(1 + \frac{1}{C_e}\right)\right\}^2\right] \tag{7}$$

Where, k_D = Dubinin-Radushkevitch model constant, q_m = maximum adsorption capacity.

Temkin model: The Temkin isotherm model describes the dynamics between adsorbate and adsorbent, presenting whether the adsorption process tends towards physisorption or chemisorption. The model form is expressed in equation (8) (Al-Fawwaz et al., 2023)

$$q_e = \left(\frac{RT}{b}\right) \ln k_T + \left(\frac{RT}{b}\right) \ln C_e \tag{8}$$

Where, b = Temkin model constant related to the heat of adsorption, k_T = Temkin isotherm constant.

2.7. Thermodynamic studies

To investigate the thermodynamics of the reaction, its spontaneity, exothermic/endothermic nature, and change in enthalpy; Gibbs' Free Energy, and Van't Hoff equation were employed (Bagbi et al., 2017; Movasaghi et al., 2019; Bazi et al., 2021; Al-Jubory et al., 2024). This study allows for a direct assessment of the influence of temperature on the adsorption process. The relation among Entropy (ΔS), Enthalpy (ΔH) and Gibbs Free Energy (ΔG) of the reaction is shown in equations (9) and (10) (Hamadeen and Elkhatib, 2022)

$$\ln K_c = \frac{\Delta S}{R} - \frac{\Delta H}{RT} \tag{9}$$

$$\Delta G = -RT \ln(K_c) \tag{10}$$

Where, $K_c = C_{ads}/C_e$, *Kc* is the distribution constant, C_{ads} is concentration of CIP adsorbed on adsorbent surface (mol/L), *Ce* is residual equilibrium concentration (mol/L), ΔS is the entropy of reaction, ΔH is the enthalpy of the system and, ΔG is the Gibb's free energy. The linear Plot of ln K_c *vs.* 1/T will help to determine the parameters such as Entropy (ΔS) and Enthalpy (ΔH).

3. Results and discussion

3.1. Characterization of biochar

3.1.1. TGA analysis of raw wheat straw (WS)

The thermal properties of wheat straw biomass were analyzed through TGA analysis. Fig. 2(a) shows the TGA and differential thermogravimetric (DTG) analysis results for the wheat straw biomass sample. TGA was conducted under nitrogen (N_2) atmosphere at a flow rate of 20 ml/min. Sample of wheat straw weighing ~5–10 mg was pyrolyzed up to a maximum temperature of 700 °C at heating rate of 10 °C/min. The TGA profiles reveal that WS biomass degrades into four stages as shown in Fig. 2(a). The moisture content present in the biomass samples is removed in the first degradation zone (25–150°C) which is due to cleavage of glycosidic groups (Mishra and Mohanty, 2020), whereas, in the second zone (150–450 °C), the maximum biomass has been converted to biochar material that happens due to depolymerization of cellulose into anhydro-oligosaccharides and anhydro-saccharides (Pelaez-Samaniego et al., 2022). The maximum degradation temperature and end temperature of WS biomass has been recorded as 344.5 °C and 373.5 °C respectively. However, the onset temperature was recorded for two steps *i.e.* 212.5 °C and 285.5 °C respectively. The peak temperature in the DTG curve determined the maximum reaction rate. Moreover, decomposition of hemicellulose, cellulose and lignin has been observed at 225–325 °C, 325–375 °C, and 417–607 °C, respectively

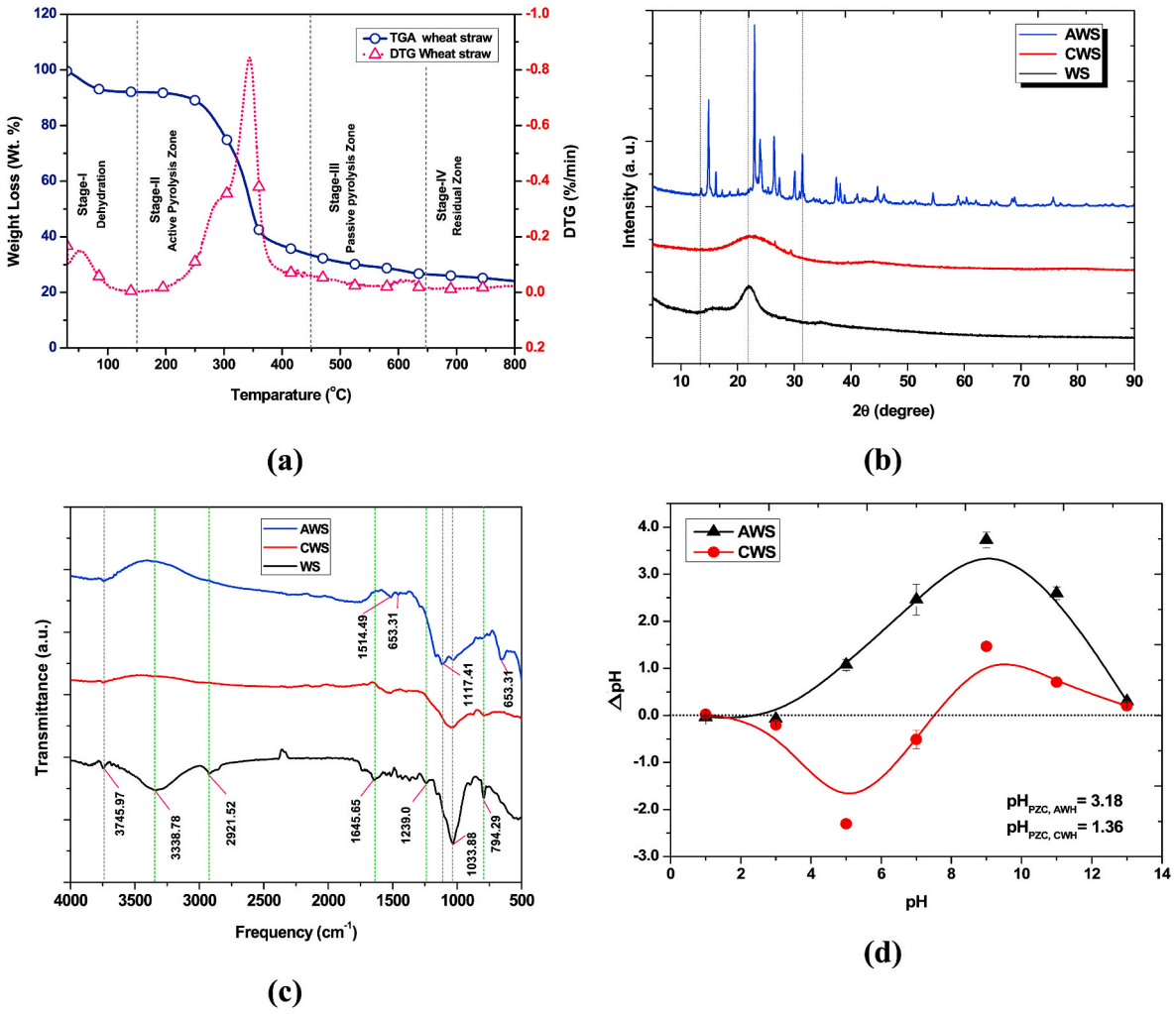

Fig. 2. Characterization of Biochar **(a)** TGA and DTG Analysis of wheat straw (WS) biomass, (b) XRD analysis of WS, CWS and AWS, **(c)** FTIR analysis of WS, CWS and AWS, (d) pH_{pzc} of CWS and AWS adsorbents.

(Mishra and Mohanty, 2020). The formation of peaks at 285 °C and 344 °C corresponds to hemicellulose and cellulose degradation, respectively. However, the decomposition of lignin reported broader degradation range and found up to 900 °C (Yang et al., 2007; Pelaez--Samaniego et al., 2022). Lignin pyrolysis is more complex than that of cellulose and hemicellulose due to its intricate structure. Consequently, lignin produces a higher yield of char compared to cellulose and hemicellulose.

3.1.2. *Powder X-ray diffraction spectrum*

The crystallographic characteristics of biomass and biochar samples were determined using powder XRD and the results are shown in Fig. 2 (b). The XRD peak at 21.89° reveals the presence of SiO_2 in the WS biomass samples as an amorphous form as depicted (Ramasamy et al., 2023). However, calcined biomass and activated biomass samples have other peaks as well. The CWS biochar sample consists of 21.2°, 26.6° and 29.4° peaks, which represent the existence of SiO_2 (amorphous) and $CaCO_3$ (Hernández-Escobar et al., 2023). Moreover, H_3PO_4 activated biochar (AWS) consists of peaks at 14.8°, 16.2°, 22.9°, 23.9°, 26.4°, 30.1°, 31.4°, 37.3°, 38.1°, 44.6°, 54.4°, 58.8°, 60.4°, 68.8°, and 75.7°. The XRD peaks detected at 2θ of 14.8° and 23.9° in the case of AWS biochar correspond to the (101) and (002) facets, indicating the crystalline structure and amorphous carbon, respectively (Buazar, F., 2019; Nguyen et al., 2023a). The peaks at 2θ from 26.4 to 31.4° suggested the existence of crystalline SiO_2 (Nguyen et al., 2023a). Also, the peaks at 37.3, 54.5, and 68.8 represent the presence of CaO in the biochar sample, while peaks at 42.1°, 42.5° and 62.1° represent the presence of MgO (JCPDS01–087-0651) as also reported in the earlier investigations (Alawa and Chakma, 2023). XRD results depict that the biomass and synthesized biochar samples are amorphous in nature, which signifies higher possibility of adsorption on their surfaces. Furthermore, the improvement in surface characteristics can influence the adsorption.

3.1.3. *Fourier transform infrared (FTIR) spectra analysis*

The functional group analysis of biomass and biochar samples was carried out using FTIR technique. The results of FTIR are shown in Fig. 2 (c). As per the analysis, biochar samples show different functional groups present in the material. The peak signal at ~3338.78 cm^{-1} represents the –OH hydroxyl functional group which dominates the presence of water, acid, phenols and aromatic compounds. The peak signal at 2921.52 cm^{-1} represents the methylene C–H *asym./sym.* stretching which is the indication of the presence of alkane ($R–CH_3$) group; however, the peak at 1645.65 cm^{-1} is credited to C═C stretch (Nandiyanto et al., 2019; Mishra and Mohanty, 2020). Furthermore, the presence of aromatics and ethers were confirmed by O-stretching at the dominated peak 1239.0 cm^{-1}. The peak at 1033.88 cm^{-1} dominates the presence of primary amine. The characteristic peak at 794.29 cm^{-1} corresponds to asymmetric stretching of Si–O–Si in the WS biomass samples (Buazar, F., 2019; Ramasamy et al., 2023). The peak signals between 700 and 1600 cm^{-1} represent the presence of cellulosic and

ligneous components (Wu et al., 2022). However, the CWS-700 shows the peaks signals and corresponding functional groups at 790.96 (C–H 1, 3-Disubstitution), 1040.17 (C–O, Si–*O*–Si), 1395.35 (O–H bend), 1515.31 (N–H bending), 1522.14 (aromatic nitro compounds), 1700 (COOH group), and 3745.97 (Si–OH groups) cm^{-1}, and AWS-700 shows the peak signals at 653.31 (C–H Bending), 753.08 (C–H 1,3-Disubstitution), 807.58 (C–H 1,3-Disubstitution), 837.0 (C–*O*–O Stretch), 1032.89 (Si–*O*–Si), 1117.41 (C–O stretching vibration), 1165.05 (C–*O*–C asymmetry stretching), 1453.96 (CO_3^{-2}), 1514.49 (N–H bending), 3740.93 cm^{-1} (Si–OH groups) respectively. Compared with the raw biomass (WS), the biochar (CWS) and activated biochar (AWS) have changed their spectra and the peaks near 2921.52 and 3338.78 cm^{-1} were found absent in both biochars. Moreover, peak shifting has been observed at peak signals 794.29 cm^{-1}, and 1033.88 cm^{-1} (Pituello et al., 2015; Liu and Fan, 2018; Nandiyanto et al., 2019; Paukshtis et al., 2019; Suman et al., 2021; Wu et al., 2022; Almanassra et al., 2024).

3.1.4. pH_{PZC} determination

The pH at the point of zero charge (pH_{pzc}) serves as a crucial determinant in understanding adsorbents' behavior, significantly impacting the adsorption process by reflecting the net surface charge in solution. The pH_{pzc} of the AWS and CWS adsorbents were established through the pH drift method (Hamadeen and Elkhatib, 2022) and depicted in Fig. 2(d). The pH_{pzc} of AWS and CWS adsorbent were found to be 3.18 and 1.36 as shown in Fig. 2(d). This explains that, at solution pH value of 3.18 and 1.36, the net charge on the AWS and CWS adsorbent surface is zero.

3.1.5. Brunauer–emmett–teller (BET) surface area analysis

The surface characteristics and porosity of the adsorbents prepared from waste agricultural biomass has been evaluated using BET surface area method. The N_2 adsorption desorption and pore volume distribution of the adsorbents is shown in Fig S1 and Table 1. As per the results, the WS adsorbent follows (Fig S1-a) type III isotherm with H3 hysteresis loop, while CWS (Fig. S1-b) and AWS (Fig. S1-c) adsorbents follow the type IV isotherm with H3 and H4 hysteresis loop respectively (Nguyen et al., 2023b). The surface area (S_{BET}) of WS biomass was found to be increased by 10 times after conversion into biochar. The increment in the surface area of the biochar was found due to the pyrolysis temperature, residence time and the type of biomass used (Alawa et al., 2024). As discussed in section 2.2, the thermal treatment of the agro-waste gives great insights towards the increment of the biochar surface and pore volumes (Ding et al., 2022; Alawa et al., 2024). However, activation with H_3PO_4 reduced the biochar surface area from 273 to 219 m^2g^{-1} (Table 1) while enhanced the pore volume and pore diameter of the biochar from 0.226 cm^3g^{-1} to 0.271 $cm^3g^{-1}$and 3.41 nm–3.81 nm respectively. The reduction in the surface area was found due to collapse of pore and excessive activation (Dechapanya and Khamwichit, 2023; Jiang et al., 2024). The conversion of biomass to biochar and activated biochar material resulted in formation of mesopores, predicting improved adsorption capacity.

3.1.6. Field emission scanning electron microscopy (FE-SEM) analysis

The surface morphology of the agro-based adsorbents has been investigated using FE-SEM analysis and the results are shown in Fig S2. The raw biomass sample shows no pores on the surface, however, CWS sample shows the change in texture of the material. WS sample shows the flaky structure. Calcination enhances the surface properties such as structure, porosity and pore volumes as also supported by the S_{BET} results (Sahoo et al., 2021; Singh et al., 2024b; Alawa et al., 2024). The acid treated biochar (AWS) shows breaking of small flakes during treatment as shown in Fig S2(c). The elemental mapping of AWS shows the presence of C, Al, Si, O and P elements. The EDX analysis further reveals the presence of oxygenated compounds on the surface of the adsorbents that was also confirmed by the FTIR analysis (Fig. 2(c)). These oxygen rich compounds change the overall adsorption efficiency of the adsorbent.

Table 1
BET surface area and pore volume distribution of the adsorbents used.

Adsorbent	S_{BET} (m^2g^{-1})	Pore Volume (cm^3g^{-1})	Pore diameter (nm)
WS	28	7.4×10^{-2}	3.41
CWS	273	2.2×10^{-1}	3.41
AWS	219	2.7×10^{-1}	3.84

4. Adsorption studies of CIP using WS derived adsorbents

4.1. Optimization of process parameters

The adsorption studies of CIP were initiated using raw biomass, *viz.* WS, followed by CWS and AWS. The optimization of the process parameters such as solution pH, adsorbent dose, contact time, initial concentration, and temperature was carried out (Singh et al., 2022), as shown in Figs. 3–4. Effect of solution pH is one of the important parameters for the adsorption studies.

4.1.1. Effect of adsorbent dose

The effect of adsorbent dose on the removal of CIP using three adsorbents (*viz.* WS, CWS, and AWS) was investigated. As per the obtained results, no adsorption has been found in the case of WS adsorbent even after increasing the dose up to 4.0 gL^{-1}. Hence, the effect of adsorbent dose on CIP removal using CWS and AWS were analyzed (Fig. 3). The results reveal that optimum adsorption is 85.22% and 98.2% in case of CWS and AWS, upon using the dose of 1.6 gL^{-1} and 1.0 gL^{-1} respectively. The AWS adsorbent is showing good adsorption characteristics towards CIP. The removal percentage of CIP by CWS and AWS adsorbents show a direct correlation with the quantity of the absorbent, with higher amounts of the adsorbent resulting in higher removal. This can be attributed to the increased availability of adsorption sites upon increasing the adsorbent's concentration (Azzam et al., 2022; Sang et al., 2022; Farzinmanesh et al., 2024).

4.1.2. Effect of solution pH

The adsorption behavior of CIP on the three prepared adsorbents *viz.* WS, CWS and AWS were investigated with respect to pH, and the findings are presented in Fig. 4(a). The variation of pH was recorded in the pH range of 1–13. CIP is an organic molecule with zwitter ion charge having two acid dissociation constants: $pKa_1 = 6.1$ (in its cationic form) and $pKa_2 = 8.7$ (in its anionic form). At pH levels below 6.09, it manifests as cationic species (CIP: +ve; protonated amine group), while at pH levels above 8.64, it may appear as anionic species (CIP: −ve; completely negatively charged). Between the pH range of 6.09–8.64, CIP exists as neutral (zwitter ionic) species (CIP: zero; zwitter ionic species with a negatively charged carboxyl group and a positively charged amine group) (Ersan et al., 2023; Jorge et al., 2024). As per the results, there is no effect of pH on the removal of CIP onto WS surface. However, in case of CWS and AWS, the removal of CIP was found to be increasing with an increase in pH from 1 to 7, after which the removal was found to be in decreasing order up to 13. Below pH 6.1, the positively charged CIP + predominates and strongly attracts the negatively charged adsorbents, resulting in the highest adsorption capacity observed at pH 5 and 7 for both AWS and CWS (as shown in Fig. 4(a)). When the pH is between pKa1 and pKa2, the zwitter ionic form (CIP±) contains both positively and negatively charged groups, which interact with AWS and CWS to facilitate adsorption. The AWS adsorbent interacts with the positively charged CIP ions in the pH range 5–7, and it shows good adsorption compared to that achieved in the pH range of 7–11. Also, presence of other functional groups (C–O, O–H, COOH, N–H) plays a vital role to enhance the adsorption through electrostatic attraction. The low adsorption of CIP in the pH range below and above 7 is due to double charged ions, which create repulsive forces among CIP molecules

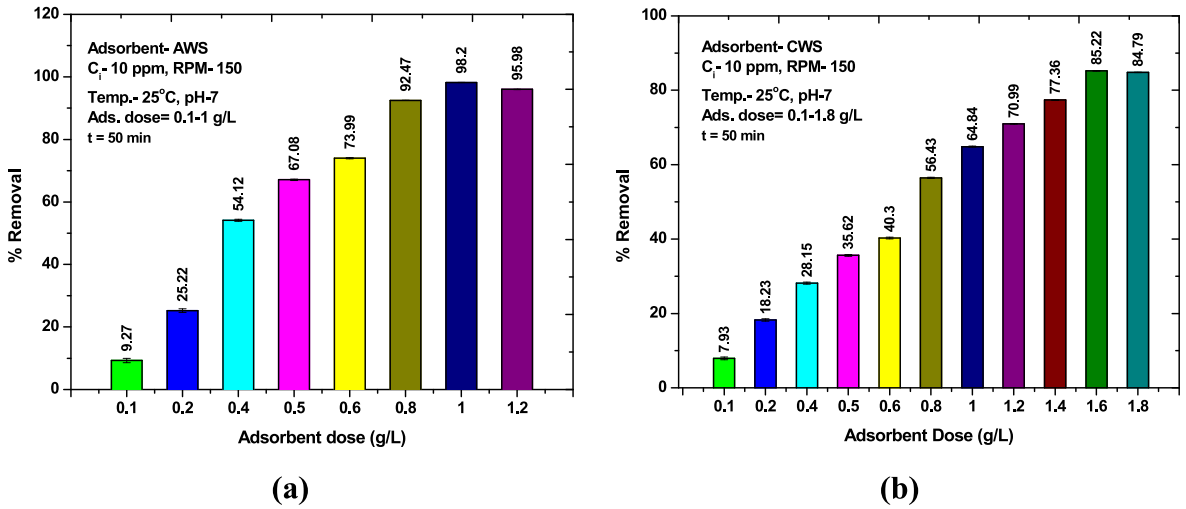

Fig. 3. Effect of adsorbent dose on adsorption of CIP using (a) (AWS) and (b) (CWS).

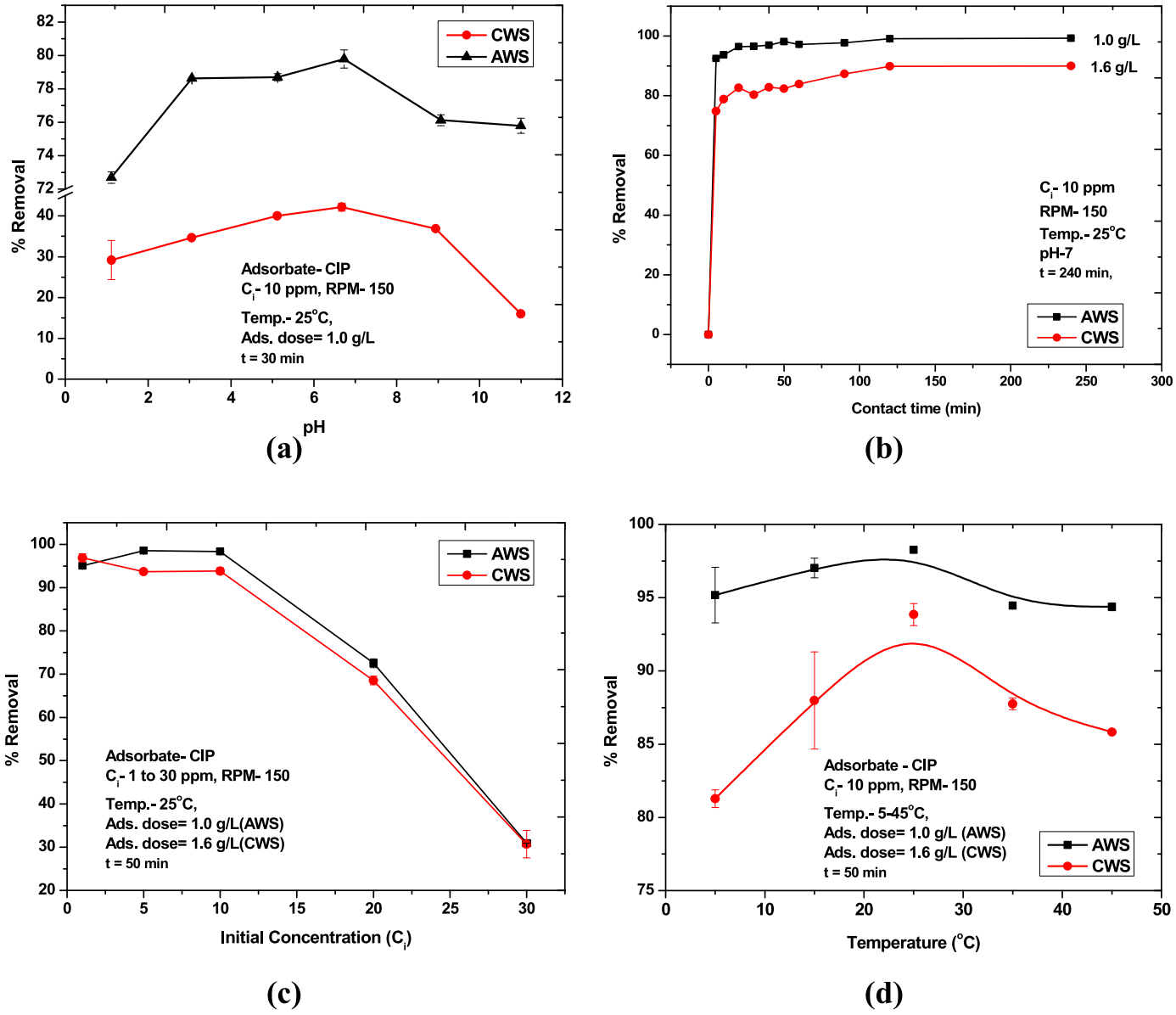

Fig. 4. Effect of various parameters on CIP adsorption **(a)** Effect of pH, **(b)** Effect of Contact time, **(c)** Effect of initial concentration, **(d)** Effect of temperature.

and surface charges of the adsorbents (Igwegbe et al., 2021; Azzam et al., 2022). The highest removal efficiency at pH 7 were found to be 42.16% and 79.78%, in the case of CWS and AWS adsorbents, respectively when used at 1.0 gL^{-1} of adsorbent dose for 30 min under room temperature conditions. Similar kinds of optimization were found by the earlier studies with different adsorbents (Ma et al., 2015; Azzam et al., 2022). Moreover, the difference in percentage removal of CIP at varying pH was less in case of AWS (*viz*. 8.8%), as compared to CWS (82.3%). This optimized pH value (*viz*. pH 7) was maintained for further experiments using the synthesized adsorbents.

4.1.3. Effect of interaction period/contact time

Fig. 4(b) illustrates the impact of contact time on the adsorption of CIP by WS, CWS and AWS. No effect was observed for the adsorption of CIP on to the WS surface as per our investigations. However, CWS and AWS resulted in significant adsorption with respect to time as shown in Fig. 4(b). The equilibrium was nearly reached within 50 min, with a slight increase in removal efficiency thereafter. It is noteworthy that CIP showed more favorable adsorption onto AWS compared to CWS, consistent with the suggested enhancement of acidity, as CIP adsorb more due to electrostatic interactions between CIP molecules and adsorbent functional groups (Xue et al., 2022). Interestingly, the removal of CIP was found to be ~92.5% and ~74.84% on AWS and CWS adsorbent surface, respectively. Thereafter, only ~5.8 and ~16.7% removal has been noticed up to reaching the equilibria in case of AWS and CWS, respectively. The maximum (98.2%) removal was observed within 50 min for AWS however, the maximum values (89.85%) attained at an equilibrium time of 120 min for CIP in the case of CWS adsorbent with 1.6 g/L of adsorbent dose. The highest removal of the CIP was found 98.2% and 89.85% in case of AWS and CWS adsorbents with optimum dose conditions, respectively.

The rapid kinetics observed within the first 5 min can be attributed to a greater number of active sites on the surfaces of AWS and CWS, available for binding with CIP in the solution. However, as time progresses, the accumulation of CIP particles on the surfaces of the adsorbents hinders the availability of free sites, leading to a slower adsorption process (Wu et al., 2019; Gubitosa et al., 2022). Similar kind of observations of rapid removal have been reported by the Wu et al. (2018) using modified Fe-MCM-41 material with 20 M ratio of Si to Fe when experiments were conducted at 5.4 pH and 175 rpm for 20 mg L^{-1} CIP solution (Wu et al., 2018). This phenomenon can be understood through the movement of CIP ions towards vacant binding sites and their distribution within the pores of the adsorbent, continuing until saturation of all active sites occurs (Xue et al., 2022; Khan et al., 2024a, 2024b).

4.1.4. Effect of initial concentration of adsorbate

The effect of initial concentration of CIP was also investigated and depicted in Fig. 4(c). As per the results, the % CIP adsorption decreases with increase in initial concentration of CIP for both the adsorbents. Also, there is a clear trend of increasing adsorption capacity with higher concentrations of CIP as shown in Fig S3. At an initial CIP concentration of 1 mgL^{-1}, the concentration at adsorption equilibrium was 0.05 mgL^{-1}, with a corresponding adsorption capacity of 0.95 mg g^{-1} for AWS. When the initial concentration was raised to 20 mgL^{-1}, the equilibrium concentration rose to 5.5 mgL^{-1}, with an increased adsorption capacity of 14.51 mgg^{-1} for AWS absorbent. The maximum adsorption capacity for CWS adsorbent was determined to be 8.56 mg g^{-1}. Results show that the activation of biochar increases the adsorption capacity by 36.31–43.59%.

4.1.5. Effect of temperature

The effect of temperature on the adsorption was investigated in the temperature range of 5–45°C, at optimum conditions. As per the obtained results, the removal efficiency has been increased with increase in temperature from 5 to 25°C for both AWS and CWS. Thereafter, the adsorption was found to decrease with an increase in temperature from 25 to 45°C as shown in Fig. 4(d). It is noteworthy that the removal of CIP lies between 94.3 and 98.2% for AWS and 81.2–93.4% for CWS adsorbent when the temperature changes from 5 to 45°C. It shows the considerable adsorption efficiency of at least ~94 and ~81% of removal of CIP at all varying temperature conditions for AWS and CWS respectively. Similar kind of trend was found by the previous studies with different adsorbents (Alnajrani and Alsager, 2020; Osman et al., 2023). It showed the complexity and challenging nature during the adsorption at different temperatures. However, CIP adsorption was found to be highest at 25°C indicating the future viability to use these prepared adsorbents for practical application in field.

4.2. Adsorption kinetics of ciprofloxacin on AWS and CWS adsorbents

To develop a robust and sustainable adsorption system, it's crucial to investigate the dynamics of the reaction, particularly the orders of the rate constants. Subsequently, adsorption kinetics data for the ciprofloxacin using AWS and CWS adsorbents was analyzed. Five kinetic models, as mentioned in section 2.5 (Table S1), were investigated and results are shown in Fig. 5 and S4-S6. In this analysis, both the linear and nonlinear fitting methods were examined. Table S2 shows the linear and nonlinear kinetic model parameters for adsorption of CIP on to AWS and CWS surface. As per the investigations, pseudo second order (PSO) gives the better fit as compared to other kinetic models for both the adsorbents with R^2 *value* of 0.999 for each, as given in Table S2. However, nonlinear intraparticle diffusion (NLIPDM) fits better in terms of calculated q_e and R^2 respectively. Moreover, activation increases the adsorption capacity from 4.70 to 9.33 mg/g as calculated by NLIPDM (Table S2).

4.3. Adsorption isotherms of ciprofloxacin on AWS and CWS adsorbents

Fig S7 (a-d) shows the linear adsorption isotherms for CIP on AWS and CWS surface. Fig. S7 (e) indicates the nonlinear adsorption isotherms (Langmuir and Freundlich) for ciprofloxacin on AWS and CWS. The detailed isotherm parameters obtained from the fitting are shown in Table S3. The comparative parameters of the isotherms revealed that CIP adsorption by AWS and CWS showed the best fit to Langmuir isotherms with higher R^2 value of 0.985 and 0.981 respectively (Fig. 5 c). This observation confirms that the adsorption of CIP on AWS and CWS adsorbents is characterized by surface adsorption, where a single layer coats homogeneous surface. Moreover, active sites exhibit consistent adsorption energy levels (Laishram et al., 2022). Additionally, using Eq. (5), R_L values were calculated as 0.036 and 0.012 for adsorption of ciprofloxacin by CWS and AWS, respectively. The Langmuir separation factor (R_L) reveals that the CWS and AWS favor the adsorption as the R_L values fall within the range 0 and 1 (Alnajrani and Alsager, 2020). As per the isotherm's investigations, CIP adsorption is primarily governed by the Langmuir isotherms for both adsorbents (CWS and AWS). This result is consistent with the previous studies (Nguyen et al., 2020; Yilmaz et al., 2022; Jiang et al., 2024).

4.4. Adsorption thermodynamics of ciprofloxacin on AWS and CWS adsorbents

The effect of temperature on the CIP adsorption using CWS and AWS biochar is shown in Fig S8. The calculated values of ΔG, ΔS, and ΔH at different temperatures are listed in Table S4. The adsorption capacity of both the adsorbents increases with an increase in temperature from 5 to 25°C, while further increase in temperature decreases the adsorption capacity. Similar kind of observation has been found for CIP adsorption using PIM (polymer intrinsic microporosity) material (Alnajrani and Alsager (2020). However, in current investigation, the reduction in adsorption capacity (Q_m) has been minimal and found to be ~4% (94.3–98.3%). As per the values of the thermodynamics parameter (range: 5–25 °C), it has been concluded that the adsorption process is endothermic and spontaneous (Fig. 5 d). Ouyang et al. (2023) also

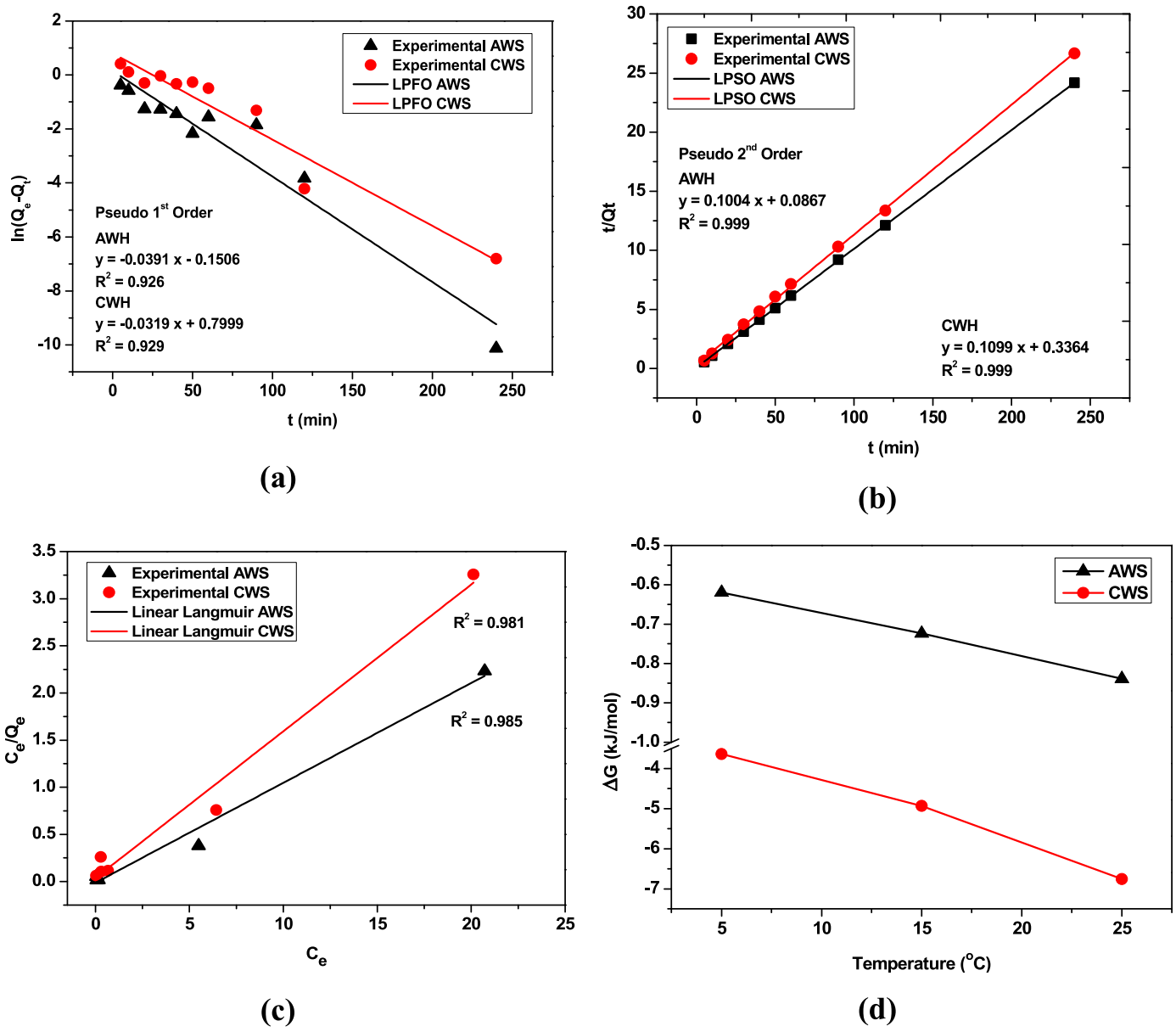

Fig. 5. Reaction kinetics (a–b), isotherm (c), and thermodynamics (d) of CIP adsorption by AWS and CWS.

showed the adsorption of CIP in the temperature range of 15–45 °C (288–318 K) and found similar observations (Ouyang et al., 2023).

5. Mechanism of CIP adsorption on biochar adsorbent

The adsorption of CIP on CWS and AWS biochar is mainly driven by a combination of physical and chemical mechanisms. The rich carbon contents (>50%) in both biochar help to increase the hydrophobic interaction between CIP aromatic ring and biochar surface. This mechanism was also supported by the thermodynamic studies (Ouyang et al., 2023; Alawa et al., 2024). The π-π stacking interactions between CIP aromatic structure and the conjugated carbon of biochar further strengthened the adsorption. As explained in section 4.1.2, CIP shows the zwitter ion characteristics having two acid dissociation constants. Below pH 6.1, the positively charged CIP + predominates and strongly attracts the negatively charged adsorbents, resulting in the highest adsorption capacity observed at pH 5 and 7 in (Fig. 4(a)). When the pH is between pKa1 and pKa2, the zwitter ionic form (CIP±) contains both positively and negatively charged groups, which can interact with adsorbents to facilitate adsorption (Pham et al., 2025). As per the findings, the pH_{PZC} of both adsorbents were found to be less than 4. Therefore, the electrostatic interactions play a significant role between pH 4–7 for better adsorption (as shown in Fig. 4(a)) (Pham et al., 2024; Le et al., 2024). Also, CIP has ionizable groups like carboxyl (–COOH) and amino ($–NH_2$), which can interact with charged functional groups on the biochar surface at different solution's pH. The presence of –OH (as discussed in section 3.1.3), nitrogen containing, and –COOH groups functional groups enhance the hydrogen bonding and promote the EDA interactions as also described by the isotherm studies (Xue et al., 2022; Barzegar et al., 2023). The improvement in surface properties after H_3PO_4 treatment enhances the adsorption capacity of AWS biochar (Fig. 6). The high surface area and high porosity of biochar provides numerous active sites, improving the overall adsorption capacity for CIP (Arif et al., 2022; Farzinmanesh et al., 2024; Jiang et al., 2024). The adsorption of biochar is not only governed by the electrostatic interaction, but also controlled by the factors such as biochar properties mesopores, non-carbonated portion, and surface functional groups. Physical adsorption occurs due to van Der Waals forces which further contribute

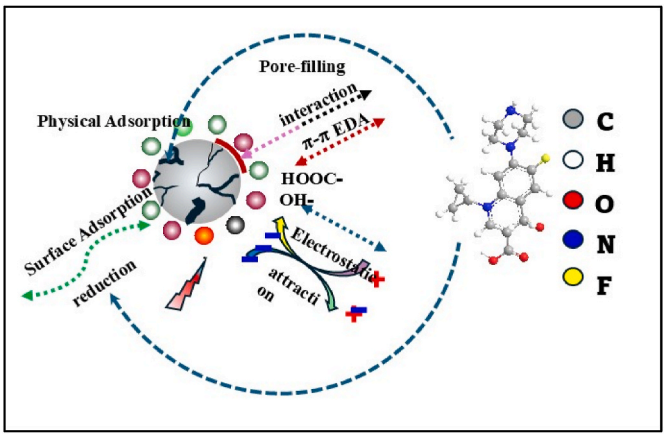

Fig. 6. Schematic representation of the possible mechanisms involved during the adsorption of CIP on to the biochar surface in aqueous medium.

to the overall adsorption of CIP.

These combined mechanisms assist wheat straw derived biochars to act as effective adsorbents for removing ciprofloxacin from aqueous environment. The developed biochar is novel in the sense that it not only helps in the removal of antibiotics from water; but it also helps in minimizing air pollution as it has been synthesized from waste material that is generally burnt. Moreover, this material was synthesized from a waste which is available in plenty and free of cost in India. The synthesized adsorbent showed promising results in minimal duration after the start of the experiment, which is significant for scale-up of the process. Further, only 0.1–1.2 g/L of the adsorbent dose was enough to achieve the ciprofloxacin removal efficiency up to 98% (Table S5).

6. Conclusion

A cost-effective adsorbent has been developed using wheat straw agricultural waste to effectively remove ciprofloxacin from water. Parametric optimization shows that the highest adsorption of CIP occurs at neutral pH, with the activated adsorbent dose of 1.0 g/L and contact time of 50 min, under ambient temperature and pressure conditions. The adsorption mechanism aligns well with the Langmuir model. Further, the adsorption process of synthesized adsorbents on CIP follows pseudo-first order and pseudo-second-order kinetics, suggesting that the adsorption mechanism is influenced by both the adsorbate and adsorbent. Study further demonstrates that activation of biochar enhances the removal of CIP by 36–45 %. The removal of CIP is mainly governed by surface and pore filling adsorption and enhanced by the electrostatic interaction between aromatic rings, hydrogen bond and surface functional groups. Thus, wheat straw derived novel adsorbent may serve as a promising candidate for removal of CIP in wastewater. The improved regeneration efficiency need to be explored further from the perspective of field-scale application and possible commercialization in future.

CRediT authorship contribution statement

Bablu Alawa: Writing – original draft, Visualization, Investigation, Formal analysis, Data curation. **Surya Singh:** Writing – review & editing, Visualization, Validation, Supervision, Project administration, Methodology, Investigation, Formal analysis, Conceptualization. **Sankar Chakma:** Writing – review & editing, Validation, Supervision, Methodology, Investigation. **Rupak Kishor:** Writing – review & editing, Validation, Methodology, Formal analysis. **Cecilia Stålsby Lundborg:** Writing – review & editing, Validation, Supervision, Resources, Project administration, Methodology, Funding acquisition. **Vishal Diwan:** Writing – review & editing, Validation, Supervision, Resources, Project administration, Methodology, Funding acquisition, Formal analysis, Conceptualization.

Funding

The authors acknowledge *Swedish Research Council, Sweden* for providing the research funding for carrying out this project (Grant No. 2021-00889).

Declaration of competing interest

The authors declare that they have no known competing financial interests or personal relationships that could have appeared to influence the work reported in this paper.

Acknowledgments

The authors are thankful to ICMR NIREH Bhopal and R D Gardi Medical College, Ujjain for providing the resources. Authors also acknowledge the cooperation provided by the local farmers (Bhauri, Bhopal, Madhya Pradesh) for allowing raw material collection.

Abbreviations:

AWS	Activated Wheat Straw
AOP	Advanced Oxidation Process
AR	Antibiotic Residues
BC	Biochar
A-BC	Activated Biochar
CWS	Calcinated Wheat Straw
CIP	Ciprofloxacin
D-R	Dubinin-Radushkevitch
EDX	Energy Dispersive X-ray spectrometer
EDA	Electron doner acceptor
FESEM	Field Emission-Scanning Electron Microscopy
FQ	Fluoroquinolones
FTIR	Fourier Transform Infrared spectroscopy
JCPDS	Joint Committee on Powder Diffraction Standards
MEUC	Microbial Electrolysis Ultraviolet Cell
NCDC	National Centre for Disease Control
PFO	Pseudo First Order
PSO	Pseudo Second Order
RPM	Round Per Minute
UV	Ultraviolet spectroscopy
WS	Wheat Straw
WHO	World Health Organization

Appendix A. Supplementary data

Supplementary data to this article can be found onlin e at https://doi.org/10.1016/j.chemosphere.2025.144252.

Data availability

Data will be made available on request.

References

Ahmad, M., Rajapaksha, A.U., Lim, J.E., Zhang, M., Bolan, N., Mohan, D., et al., 2014. Biochar as a sorbent for contaminant management in soil and water: a review. Chemosphere 99, 19–33.

Alawa, B., Chakma, S., 2023. Upgradation, product analysis and engine performance of hydrocarbon fuels produced through pyrolysis of thermoplastic polymers with Si and ZSM-5 modified catalysts. Fuel Process. Technol. 250, 107918.

Alawa, B., Singh, S., Chakma, S., Lundborg, C.S., Diwan, V., 2024. A review on utilization potential of functionalized biochar for the removal of antibiotics from water. Environ Adv, 100571.

Al-Buriahi, A.K., Al-shaibani, M.M., Mohamed, R.M.S.R., Al-Gheethi, A.A., Sharma, A., Ismail, N., 2022. Ciprofloxacin removal from non-clinical environment: a critical

review of current methods and future trend prospects. J. Water Process Eng. 47, 102725.
Al-Fawwaz, A.T., Al Shra'ah, A., Elhaddad, E., 2023. Bioremoval of methylene blue from aqueous solutions by green algae (bracteacoccus sp.) isolated from north Jordan: optimization, kinetic, and isotherm studies. Sustain. Times 15 (1), 842.
Al-Jubory, F.K., Abbas, A.S., Mujtaba, I.M., 2024. Adsorptive removal of ciprofloxacin from simulated wastewater using crosslinked starch ester: isotherms, kinetics, thermodynamics, modeling, and simulation for continuous operation. Chem. Eng. Res. Des. 200, 332–343.
Almanassra, I.W., Chatla, A., Zakaria, Y., Kochkodan, V., Shanableh, A., Laoui, T., Atieh, M.A., 2024. Palm leaves based biochar: advanced material characterization and heavy metal adsorption study. Biomass Conv Biorefinery 14 (13), 14811–14830.
Alnajrani, M.N., Alsager, O.A., 2020. Removal of antibiotics from water by polymer of intrinsic microporosity: isotherms, kinetics, thermodynamics, and adsorption mechanism. Sci. Rep. 10 (1), 794.
Arif, M., Liu, G., ur Rehman, M.Z., Yousaf, B., Ahmed, R., Mian, M.M., Ashraf, A., Munir, M.A.M., Rashid, M.S., Naeem, A., 2022. Carbon dioxide activated biochar-clay mineral composite efficiently removes ciprofloxacin from contaminated water-Reveals an incubation study. J. Clean. Prod. 332, 130079.
Azzam, A.B., Tokhy, Y.A., Farida, M., Younes, A.A., 2022. Construction of porous biochar decorated with NiS for the removal of ciprofloxacin antibiotic from pharmaceutical wastewaters. J. Water Process Eng. 49, 103006.
Bagbi, Y., Sarswat, A., Mohan, D., Pandey, A., Solanki, P.R., 2017. Lead and chromium adsorption from water using L-cysteine functionalized magnetite (Fe3O4) nanoparticles. Sci. Rep. 7 (1), 7672.
Barzegar, G., Sabaghan, M., Azadbakht, O., Aghayani, E., Mahdavianpour, M., Kadier, A., Fallahizadeh, S., Ghanbari, F., 2023. Ciprofloxacin degradation by catalytic activation of monopersulfate using Mn–Fe oxides: performance and mineralization. Water Sci. Technol. 87 (5), 1029–1042.
Bazi, M., Balarak, D., Khatibi, A.D., Siddiqui, S.H., Mostafapour, F.K., 2021. Investigation of isotherm, kinetics and thermodynamics of ciprofloxacin adsorption by molecularly imprinted polymer from aqueous solutions. Int J Pharma Inves 11 (3).
Bilal, M., Mehmood, S., Rasheed, T., Iqbal, H.M., 2020. Antibiotics traces in the aquatic environment: persistence and adverse environmental impact. Curr Opin Environ Sci Health 13, 68–74.
Buazar, F., 2019. Impact of biocompatible nanosilica on green stabilization of subgrade soil. Sci. Rep. 9 (1), 15147.
Dechapanya, W., Khamwichit, A., 2023. Biosorption of aqueous Pb (II) by H3PO4-activated biochar prepared from palm kernel shells (PKS). Heliyon 9 (7), e17250.
Ding, C., Gan, Y., Luo, J., Cui, Y., 2022. Wheat straw biochar and its performance in treatment of phenanthrene containing water and microbial remediation of phenanthrene contaminated soil. Front. Environ. Sci. 10, 1039603.
Dolfini, N., Araujo, C.M.B.D., Pereira, N.C., 2024. Amoxicillin removal from water by adsorption on activated carbon of mineral sources: discussion of experimental data, mechanisms and modeling. Environ. Technol. 45 (8), 1636–1650.
Ersan, G., Dos Santos, A.J., Lanza, M.R., Perreault, F., Garcia-Segura, S., 2023. Enhancing the selective ciprofloxacin adsorption in urine matrices through the metal-doping of carbon sorbents. J. Environ. Manag. 348, 119298.
Farzinmanesh, O., Sabzevari, M.H., Asghariganjeh, M.R., 2024. Efficient removal of ciprofloxacin and ofloxacin from aqueous solutions using a novel nano-scale adsorbent: modeling, optimization, and characterization. Chemosphere 354, 141640.
Feng, D., Guo, D., Zhang, Y., Sun, S., Zhao, Y., Shang, Q., Sun, H., Wu, J., Tan, H., 2021. Functionalized construction of biochar with hierarchical pore structures and surface O-/N-containing groups for phenol adsorption. Chem. Eng. J. 410, 127707.
Gahrouei, A.E., Vakili, S., Zandifar, A., Pourebrahimi, S., 2024. From wastewater to clean water: recent advances on the removal of metronidazole, ciprofloxacin, and sulfamethoxazole antibiotics from water through adsorption and advanced oxidation processes (AOPs). Environ. Res., 119029
Govardhan, G., Ambulkar, R., Kulkarni, S., Vishnoi, A., Yadav, P., Choudhury, B.A., Khare, M., Ghude, S.D., 2023. Stubble-burning activities in north-western India in 2021: contribution to air pollution in Delhi. Heliyon 9, e16939.
Gubitosa, J., Rizzi, V., Cignolo, D., Fini, P., Fanelli, F., Cosma, P., 2022. From agricultural wastes to a resource: kiwi Peels, as long-lasting, recyclable adsorbent, to remove emerging pollutants from water. The case of Ciprofloxacin removal. Sustain Chem Pharma 29, 100749.
Hamadeen, H.M., Elkhatib, E.A., 2022. New nanostructured activated biochar for effective removal of antibiotic ciprofloxacin from wastewater: adsorption dynamics and mechanisms. Environ. Res. 210, 112929.
Hernández-Escobar, C.A., Conejo-Dávila, A.S., Vega-Rios, A., Zaragoza-Contreras, E.A., Farias-Mancilla, J.R., 2023. Study of Geopolymers obtained from wheat husk native to northern Mexico. Mater 16 (5), 1803.
Hutchings, M.I., Truman, A.W., Wilkinson, B., 2019. Antibiotics: past, present, and future. Curr Opin Microbio 51, 72–80.
Igwegbe, C.A., Oba, S.N., Aniagor, C.O., Adeniyi, A.G., Ighalo, J.O., 2021. Adsorption of ciprofloxacin from water: a comprehensive review. J. Ind. Eng. Chem. 93, 57–77.
Jara-Cobos, L., Peñafiel, M.E., Montero, C., Menendez, M., Pinos-Vélez, V., 2023. Ciprofloxacin removal using pillared clays. Water 15 (11), 2056.
Jiang, H., Li, X., Bai, J., Pan, W., Luo, Z., Dai, Y., 2024. Removal of ciprofloxacin lactate by phosphoric acid activated biochar: urgent consideration of new antibiotics for human health. Chem. Eng. Sci. 283, 119403.
Jorge, N.L., Garrafa, M.V., Romero, J.M., Jorge, M.J., Jorge, L.C., Delfino, M.R., Meruvia-Rojas, Y.V., Hernández-Laguna, A., Sainz-Díaz, C.I., 2024. Adsorption of ciprofloxacin on clay minerals in argentinian santa rosa-corrientes soils. Molecules 29 (8), 1760.
Khan, A.H., Aziz, H.A., Palaniandy, P., Naushad, M., Zouli, N., 2024a. Ciprofloxacin adsorption onto CNT loaded Pumice: adsorption Modelling, kinetics, equilibriums and reusability studies. J. Mol. Liq. 399, 124388.
Khan, P., Saha, R., Halder, G., 2024b. Towards sorptive eradication of pharmaceutical micro-pollutant ciprofloxacin from aquatic environment: a comprehensive review. Sci. Total Environ., 170723
Kusworo, T.D., Kumoro, A.C., Puspa, M.B., Citradhitya, P., Utomo, D.P., 2024. Removal of ciprofloxacin-humic acid pollutant residue in wastewater through a hybrid treatment system consisting of pre-treatment with ozonation-AC/TiO_2/CeO_2 adsorption and degradation using PVDF/Ni-CeO2@ SiO_2 photocatalytic membrane. J. Environ. Chem. Eng. 12 (2), 112216.
Laishram, D., Kumar, D., Kant, V., Saini, B., Shejale, K.P., Krishnapriya, R., Janu, V.C., Singhal, R., Sharma, R.K., 2022. Activated hollow and solid carbon spheres for enhanced removal efficiency of pharmaceutical pollutants and heavy metals in water. Water Air Soil Pollut. 233 (10), 404.
Lan, R., Easthem, S.D., Liu, T., Norford, L.K., Barrett, S.R.H., 2022. Air quality impacts of crop residue burning in India and mitigation alternatives. Nat. Commun. 13, 6537.
Le, T.M.D., Dinh, T.D., Tran, T.M.H., Nguyen, M.K., Hoang, H., Vu, L.K., Vu, N.D.Q., Pham, T.D., 2024. Adsorption characteristics of individual and binary mixtures of ciprofloxacin antibiotic and Cu(II) on nanosilica in water. J. Mol. Liq. 398, 124298.
Leng, L., Xiong, Q., Yang, L., Li, H., Zhou, Y., Zhang, W., Jiang, S., Li, H., Huang, H., 2021. An overview on engineering the surface area and porosity of biochar. Sci. Total Environ. 763, 144204.
Liu, L., Fan, S., 2018. Removal of cadmium in aqueous solution using wheat straw biochar: effect of minerals and mechanism. Environ. Sci. Pollut. Res. 25, 8688–8700.
López-Luna, J., Ramírez-Montes, L.E., Martinez-Vargas, S., Martínez, A.I., Mijangos-Ricardez, O.F., González-Chávez, M.D.C.A., Carrillo-González, R., Solís-Domínguez, F.A., Cuevas-Díaz, M.D.C., Vázquez-Hipólito, V., 2019. Linear and nonlinear kinetic and isotherm adsorption models for arsenic removal by manganese ferrite nanoparticles. SN Appl. Sci. 1, 1–19.
Ma, J., Yang, M., Yu, F., Zheng, J., 2015. Water-enhanced removal of ciprofloxacin from water by porous graphene hydrogel. Sci. Rep. 5 (1), 13578.
Mishra, R.K., Mohanty, K., 2020. Kinetic analysis and pyrolysis behaviour of waste biomass towards its bioenergy potential. Bioresour. Technol. 311, 123480.
Movasaghi, Z., Yan, B., Niu, C., 2019. Adsorption of ciprofloxacin from water by pretreated oat hulls: equilibrium, kinetic, and thermodynamic studies. Ind. Crop. Prod. 127, 237–250.
Nandiyanto, A.B.D., Oktiani, R., Ragadhita, R., 2019. How to read and interpret FTIR spectroscope of organic material. Indonesian J Sci Technol 4 (1), 97–118.
NCDC, 2023. National AMR Surveillance Network (NARS-Net), n.d. Annual Report 2023: Ministry of Health and Family Welfare. Available at https://ncdc.mohfw.gov.in/wp-content/uploads/2024/03/1257263841692628161.pdf.
Nguyen, H.T., Van, T.N., Thi, P.N., Lan, P.D.T., Pham, H.T., Cao, H.T., 2020. Low-cost hydrogel derived from agro-waste for veterinary antibiotic removal: optimization, kinetics, and toxicity evaluation. Environ. Technol. Innov. 20, 101098.
Nguyen, T.B., Chen, W.H., Chen, C.W., Bui, X.T., Patel, A.K., Dong, C.D., 2023b. Hydrothermal and pyrolytic conversion of sunflower seed husk into novel porous biochar for efficient adsorption of tetracycline. Bioresour. Technol. 373, 128711.
Nguyen, T.B., Chen, W.H., Chen, C.W., Patel, A.K., Bui, X.T., Chen, L., Singhania, R.R., Dong, C.D., 2023a. Phosphoric acid-activated biochar derived from sunflower seed husk: selective antibiotic adsorption behavior and mechanism. Bioresour. Technol. 371, 128593.
Oharisi, O.O.L., Ncube, S., Nyoni, H., Madikizela, M.L., Olowoyo, O.J., Maseko, B.R., 2023. Occurrence and prevalence of antibiotics in wastewater treatment plants and effluent receiving rivers in South Africa using UHPLC-MS determination. J. Environ. Manag. 345, 118621.
Oliveira, M.G., Spaolonzi, M.P., Duarte, E.D., Costa, H.P., da Silva, M.G., Vieira, M.G., 2023. Adsorption kinetics of ciprofloxacin and ofloxacin by green-modified carbon nanotubes. Environ. Res. 233, 116503.
One Health Trust, 2015. Global livestock antibiotic use expected to increase 67% by 2030. One Health Trust. https://onehealthtrust.org/blog/posts/global_livestock_antibiotic_use_expected_increase_67_2030/. Nov. 13th, 2024.
Osman, D., Uyanık, İ., Mıhçıokur, H., Özkan, O., 2023. Evaluation of ciprofloxacin (CIP) and clarithromycin (CLA) adsorption with weathered PVC microplastics. J. Environ. Sci. Health, Part A 58 (5), 498–505.
Ouyang, J., Chen, J., Chen, W., Zhou, L., Cai, D., Ren, C., 2023. H3PO4 activated biochars derived from different agricultural biomasses for the removal of ciprofloxacin from aqueous solution. Particuology 75, 217–227.
Parashar, V., Singh, S., Purohit, M.R., Tamhankar, A.J., Singh, D., Kalyanasundaram, M., Lundborg, C.S., Diwan, V., 2022. Utility of constructed wetlands for treatment of hospital effluent and antibiotic resistant bacteria in resource limited settings: a case study in Ujjain, India. Water Environ. Res. 94, e10783.
Paukshtis, E.A., Yaranova, M.A., Batueva, I.S., Bal'zhinimaev, B.S., 2019. A FTIR study of silanol nests over mesoporous silicate materials. Micropor Mesopor Materials 288, 109582.
Pelaez-Samaniego, M.R., Mood, S.H., Garcia-Nunez, J., Garcia-Perez, T., Yadama, V., Garcia-Perez, M., 2022. Biomass Carbonization Technologies. Sustainable Biochar for Water and Wastewater Treatment, pp. 39–92.
Peñafiel, M.E., Matesanz, J.M., Vanegas, E., Bermejo, D., Mosteo, R., Ormad, M.P., 2021. Comparative adsorption of ciprofloxacin on sugarcane bagasse from Ecuador and on commercial powdered activated carbon. Sci. Total Environ. 750, 141498.
Pham, T.D., Nguyen, D.T., Nguyen, H.L., Nguyen, M.Q., Tran, T.M., Nguyen, M.V., Nguyen, T.L., Ngo, T.M.V., Namakamura, K., Tsubota, T., 2025. Adsorption characteristics of ciprofloxacin and naproxen from aqueous solution using bamboo biochar. Biomass Conver and Biorefinery 15, 3071–3082.

Pham, T.D., Nguyen, P.T., Phan, T.M.N., Dinh, T.D., Tran, T.M.H., Nguyen, M.K., Hoang, T.H., Srivastav, A.L., 2024. Highly adsorptive removal of ciprofloxacin and *E. coli* inactivation using amino acid tryptophan modified nano-gibbsite. Environ. Res. 258, 119396.

Pituello, C., Francioso, O., Simonetti, G., Pisi, A., Torreggiani, A., Berti, A., Morari, F., 2015. Characterization of chemical–physical, structural and morphological properties of biochars from biowastes produced at different temperatures. J Soils Sed 15, 792–804.

Qalyoubi, L., Al-Othman, A., Al-Asheh, S., 2022. Removal of ciprofloxacin antibiotic pollutants from wastewater using nano-composite adsorptive membranes. Environ. Res. 215, 114182.

Ramasamy, S.P., Veeraswamy, D., Ettiyagounder, P., Arunachalam, L., Devaraj, S.S., Krishna, K., Oumabady, S., Sakrabani, R., 2023. New insights into method development and characterization of amorphous silica from wheat straw. Silicon 15 (12), 5049–5063.

Ricky, R., Shanthakumar, S., 2023. An investigation on removal of ciprofloxacin and norfloxacin by phycoremediation with an emphasis on acute toxicity and biochemical composition. Sci. Rep. 13 (1), 13911.

Saadi, R., Saadi, Z., Fazaeli, R., Fard, N.E., 2015. Monolayer and multilayer adsorption isotherm models for sorption from aqueous media. Kor. J. Chem. Eng. 32, 787–799.

Sahoo, K., Kumar, A., Chakraborty, J.P., 2021. A comparative study on valuable products: bio-oil, biochar, non-condensable gases from pyrolysis of agricultural residues. J of Mat Cycl Waste Manage 23, 186–204.

Sang, F., Yin, Z., Wang, W., Almatrafi, E., Wang, Y., Zhao, B., Gong, J., Zhou, C., Zhang, C., Zeng, G., Song, B., 2022. Degradation of ciprofloxacin using heterogeneous Fenton catalysts derived from natural pyrite and rice straw biochar. J. Clean. Prod. 378, 134459.

Singh, V.P., Jha, D., Rehman, B.U., Dhayal, V.S., Dhar, M.S., Sharma, N., 2024a. A mini-review on the burden of antimicrobial resistance and its regulation across one health sectors in India. J Agri Food Res, 100973.

Singh, S., Lundborg, C.S., Diwan, V., 2022. Factors influencing the adsorption of antibiotics onto activated carbon in aqueous media. Water Sci. Technol. 86, 2260–2269.

Singh, R., Naik, D.V., Dutta, R.K., Kanaujia, P.K., 2024b. High surface area biochar for the removal of naphthenic acids from environmental water and industrial wastewater. Environ. Sci. Pollut. Res. 1–19.

Suliman, W., Harsh, J.B., Abu-Lail, N.I., Fortuna, A.M., Dallmeyer, I., Garcia-Pérez, M., 2017. The role of biochar porosity and surface functionality in augmenting hydrologic properties of a sandy soil. Sci. Total Environ. 574, 139–147.

Suman, S., Yadav, A.M., Jain, T., Sk, A.A., 2021. Study in the changes on the functional groups present in biomass during pyrolysis process. IOP Conf. Ser. Mater. Sci. Eng. 1146 (1), 012023. IOP Publishing.

Venkatachalam, C.D., Sekar, S., Sengottian, M., Ravichandran, S.R., Bhuvaneshwaran, P., 2023. A critical review of the production, activation, and morphological characteristic study on functionalized biochar. J Ener Storage 67, 107525.

Wang, Y., Zhu, G., Qin, L., Huang, S., 2020. Removal of antibiotics from water using biochar: a review. Chemosphere 260, 127628.

WHO, 2024. WHO reports widespread overuse of antibiotics in patients hospitalized with COVID-19. https://www.who.int/news/item/26-04-2024-who-reports-widespread-overuse-of-antibiotics-in-patients–hospitalized-with-covid-19.

Wu, M., Zhao, S., Jing, R., Shao, Y., Liu, X., Lv, F., Hu, X., Zhang, Q., Meng, Z., Liu, A., 2019. Competitive adsorption of antibiotic tetracycline and ciprofloxacin on montmorillonite. Appl. Clay Sci. 180, 105175.

Wu, S., Cai, X., Liao, Z., He, W., Shen, J., Yuan, Y., Ning, X., 2022. Redox properties of nano-sized biochar derived from wheat straw biochar. RSC Adv. 12 (18), 11039–11046.

Wu, Y., Tang, Y., Li, L., Liu, P., Li, X., Chen, W., Xue, Y., 2018. The correlation of adsorption behavior between ciprofloxacin hydrochloride and the active sites of Fe-doped MCM-41. Front. Chem. 6, 17.

Xue, Y., Guo, Y., Zhang, X., Kamali, M., Aminabhavi, T.M., Appels, L., Dewil, R., 2022. Efficient adsorptive removal of ciprofloxacin and carbamazepine using modified pinewood biochar–A kinetic, mechanistic study. Chem. Eng. J. 450, 137896.

Yang, H., Yan, R., Chen, H., Lee, D.H., Zheng, C., 2007. Characteristics of hemicellulose, cellulose and lignin pyrolysis. Fuel 86 (12–13), 1781–1788.

Yilmaz, M., Al-Musawi, T.J., Saloot, M.K., Khatibi, A.D., Baniasadi, M., Balarak, D., 2022. Synthesis of activated carbon from Lemna minor plant and magnetized with iron (III) oxide magnetic nanoparticles and its application in removal of Ciprofloxacin. Biomass Convers Biorefinery 1–14.

Yu, M., Han, Y., Tang, Y., Ma, H., 2020. Biochar for pharmaceutical contaminants removal: current status and challenges. Sci. Total Environ. 714, 136780.